Electronic Supplementary Material (ESI) for RSC Advances.

Supporting Information for

A Low-Temperature Sintered Heterostructure Solid Film of Coordination Polymer Nanoparticles: An Electron-Rectifier Function Based on Partially Oxidised/Reduced Conductor Phases of Prussian Blue

Kenta Ono, Manabu Ishizaki,* Shinobu Soma, Katsuhiko Kanaizuka, Takanari Togashi, and Masato Kurihara*

Faculity of science, Yamagata University. 1-4-12 Kojirakawa-machi, 990-8560 Yamagata, Japan.

*E-mail: kurihara@sci.kj.yamagata-u.ac.jp, manabu-ishizaki@sci.kj.yamagata-u.ac.jp

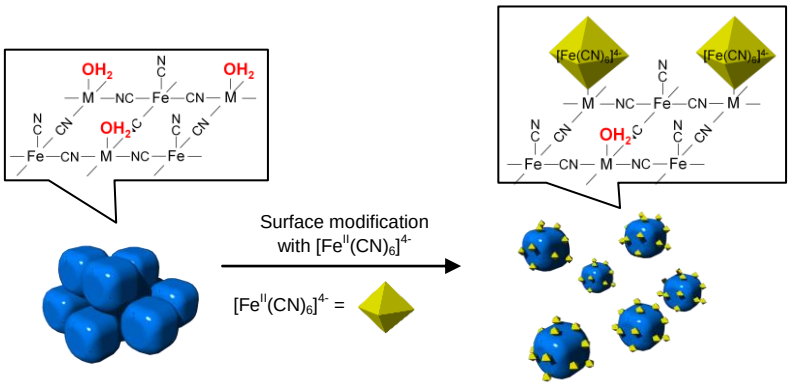

Fig. S1. A schematic image for surface modification of the PB and Ni-PBA NPs using ferrocyanide ions, $[Fe^{II}(CN)_6]^{4-}$. In the crystal lattice, the Fe-CN-M distance of the PB and Ni-PBA is approximately 0.5 nm. In an ideal 10-nm nanocube of PB or Ni-PBA, the surface M–OH_2 sites occupy 15%, numerically, of all metal ions. In this study, 70% of surface M–OH_2 sites are covered by $[Fe(CN)_6]^{4-}$.

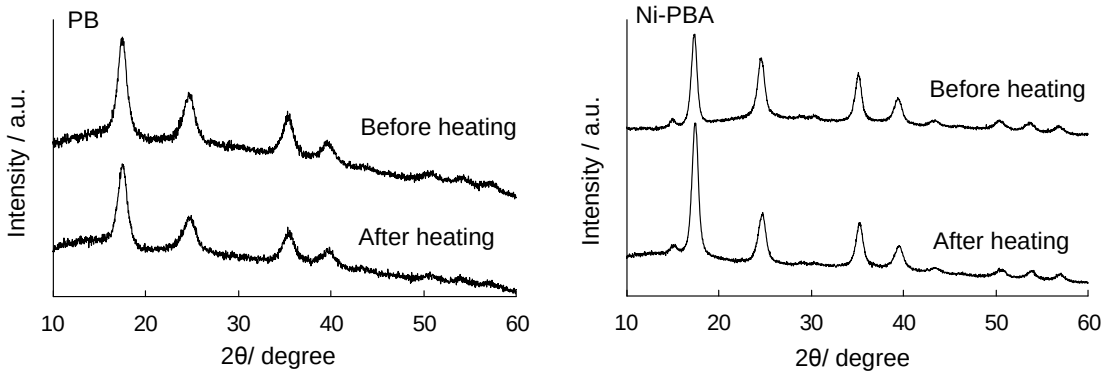

Fig. S2. XRD patterns of the PB and Ni-PBA NPs before and after heating at 150 °C.

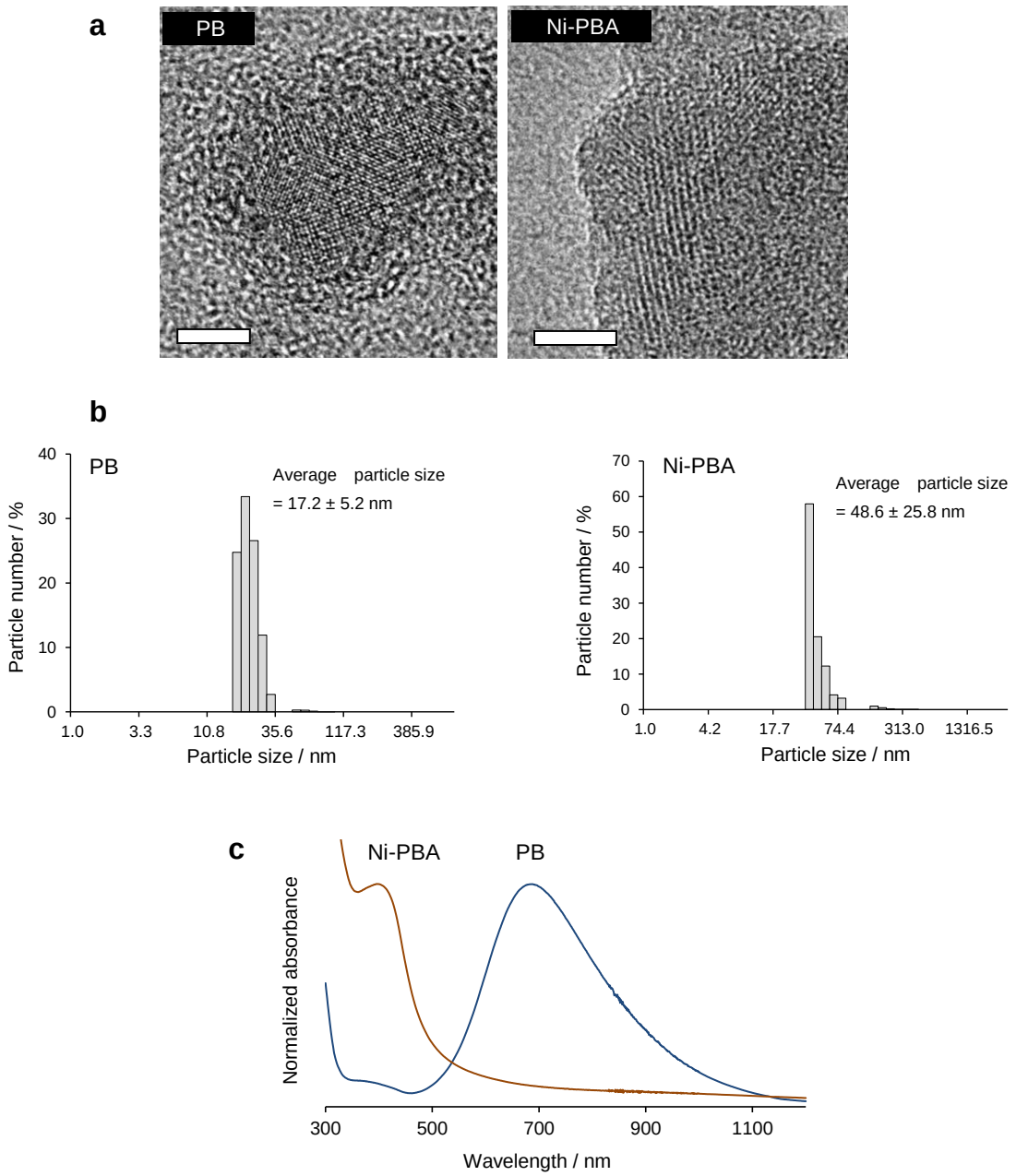

Fig. S3. Characterisation of the PB and Ni-PBA NPs and its inks. (a) High-resolution TEM images of PB and Ni-PBA NPs. The scale bars are 5 nm. (b) Number-averaged dynamic light-scattering (DLS) particle-size distributions of PB NPs and Ni-PBA NPs in their inks. The number-averaged DLS particle sizes of the PB and Ni-PBA NPs were 17 ± 5 and 49 ± 26 nm, respectively, indicating that the NPs were partially aggregated as secondary particles dispersible in water. (c) UV-Vis-NIR absorption spectra of the PB and Ni-PBA NP inks.

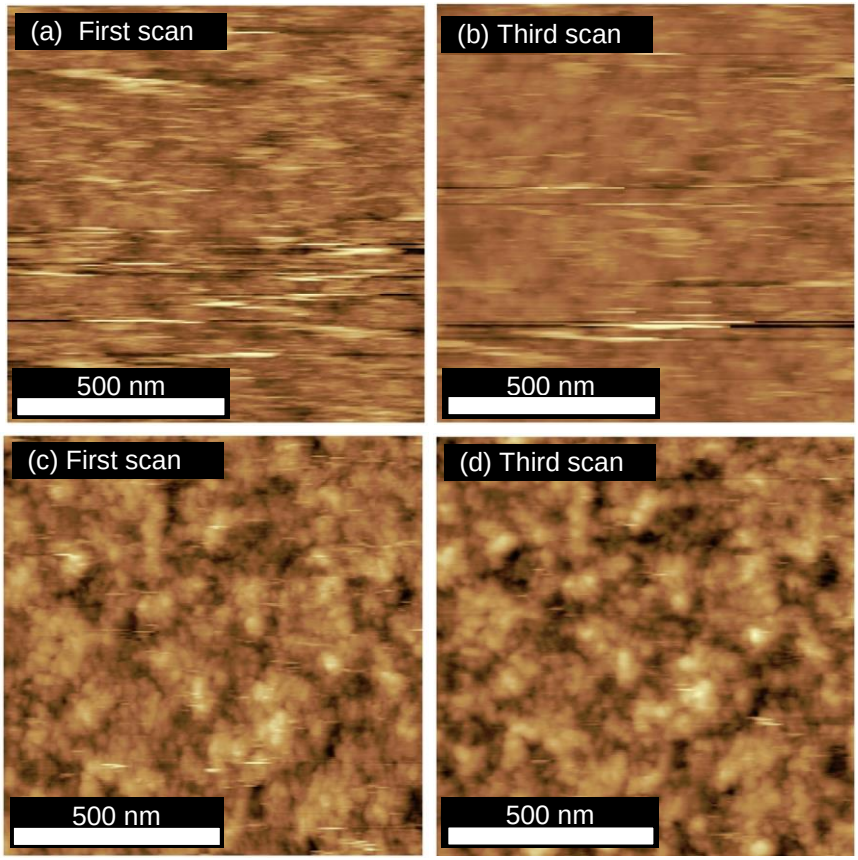

Fig. S4. AFM images (contact mode) of the PB NP film (thickness, 20 nm) before (a, b) and after sintering (c, d) at 150 °C. Scanning conditions: operation point = 0.5 V, P gain = 0.001, I gain = 500.

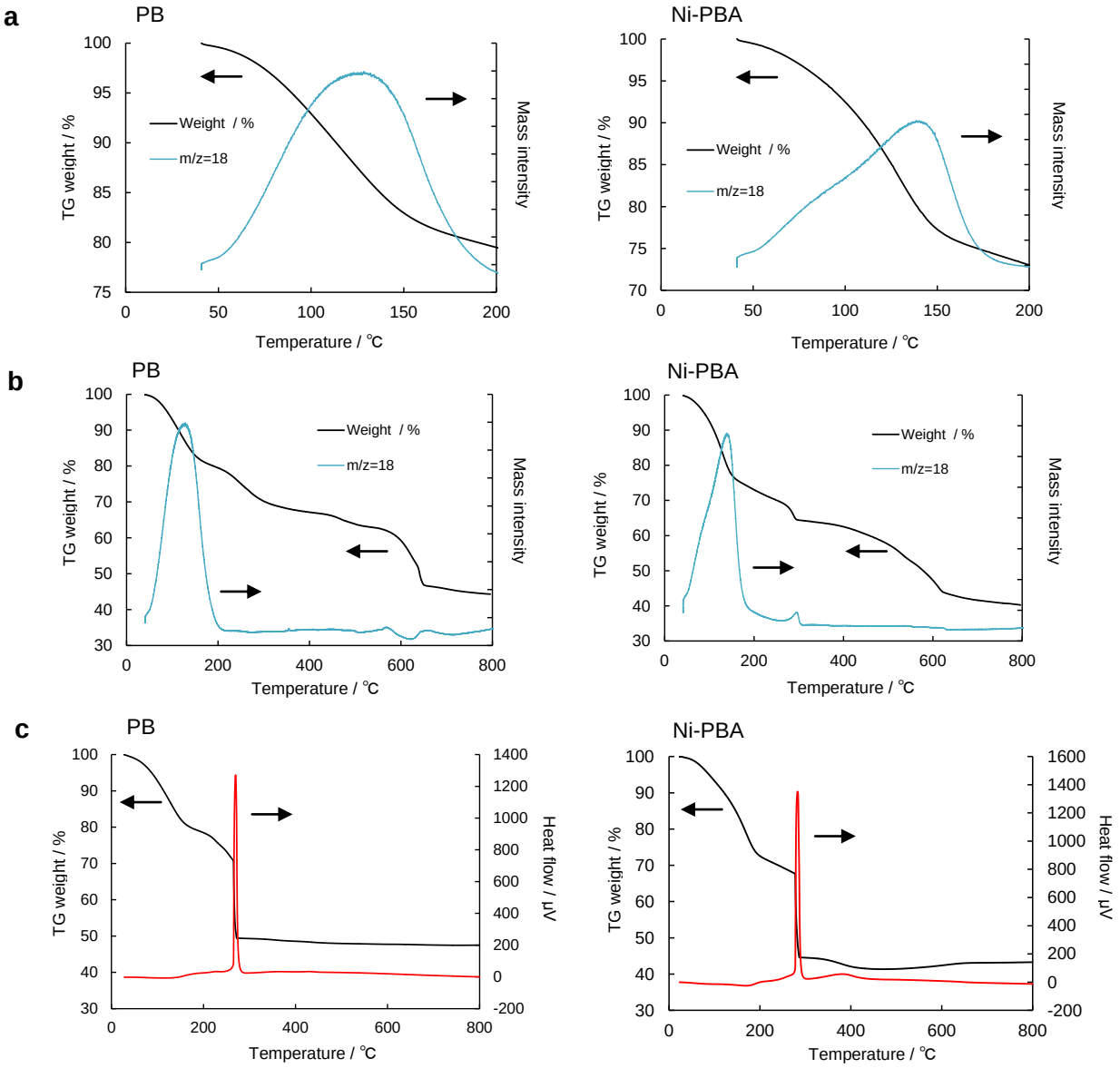

Fig. S5. Thermogravimetric analyses (TG) of PB NPs and Ni-PBA NPs (a) from 40 to 200 °C and (b) from 40 to 800 °C under a stream of He. The liberated water molecules synchronised with the TG weight loss was detected *via* the mass analysis. (c) Thermogravimetric-differential thermal analyses (TG-DTA) of PB NPs and Ni-PBA NPs from 25 to 800 °C under a stream of air. The coordination and crystal water molecules of the PB and Ni-PBA NPs are released up to 200 °C, and the PB and Ni-PBA NPs undergo exothermic decomposition at 250-300 °C under a stream of air. Decomposition of the PB and Ni-PBA NPs moderately occurs over 250 °C under a stream of the inert gas, He.

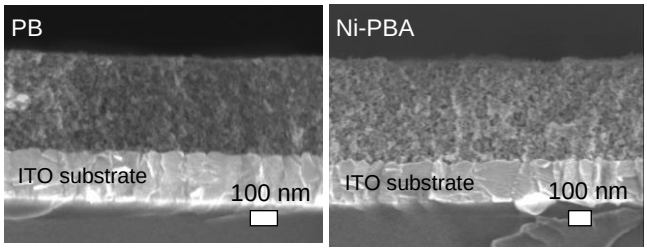

Fig. S6. SEM cross-section images of the low-temperature sintered single-layer (SL) films at 150 °C of the PB NPs (thickness, 340 nm) and Ni-PBA NPs (410 nm).

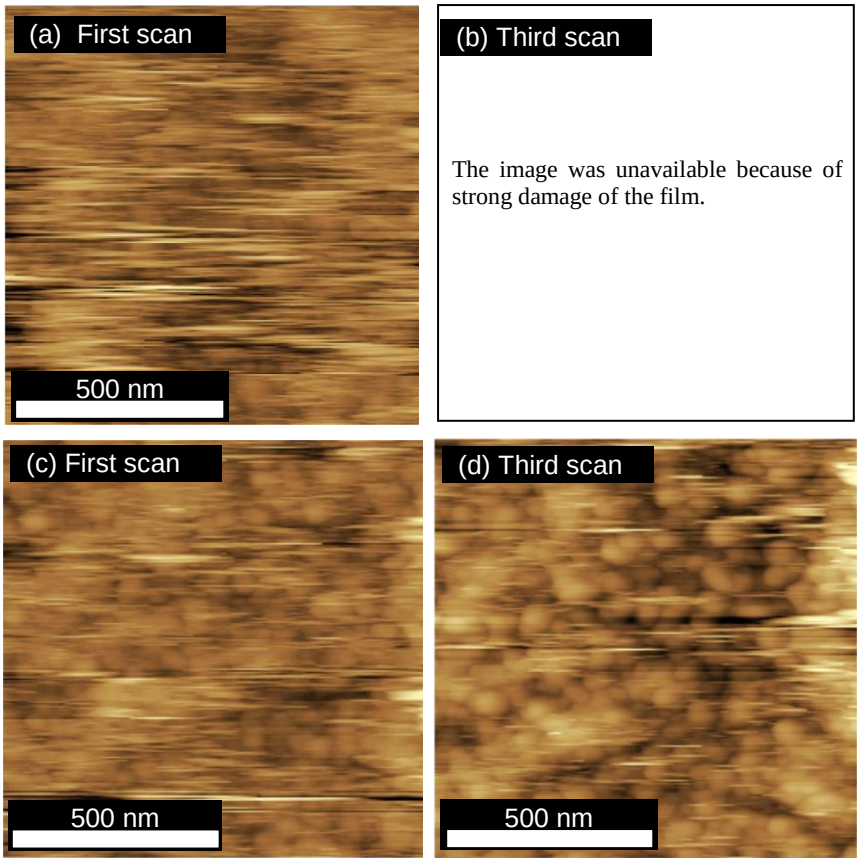

Fig. S7. AFM images (contact mode) of the Ni-PBA film (thickness, 60 nm) (a, b) before and (c, d) after sintering at 150 °C. Scanning conditions: operation point = 0.5 V, P gain = 0.001, I gain = 500.

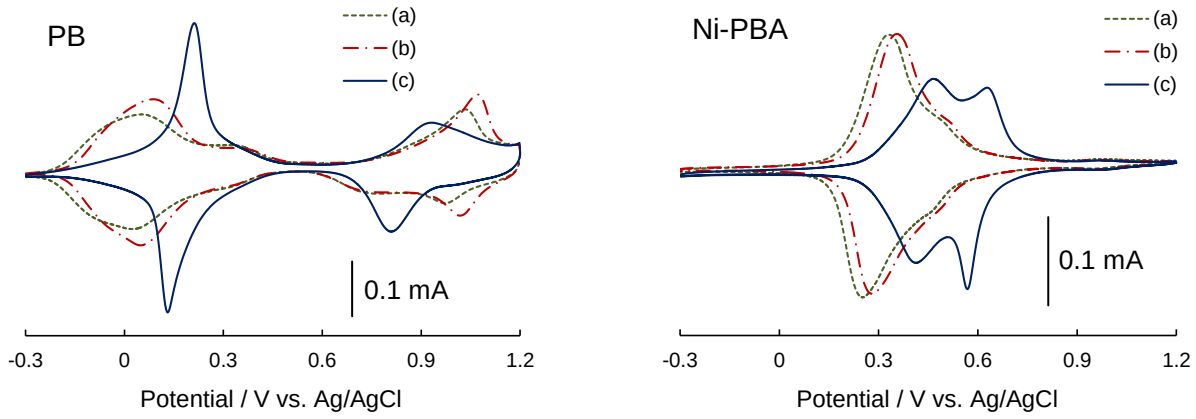

Fig. S8. Cyclic voltammograms of the low-temperature sintered SL films at 150 °C of PB and Ni-PBA NPs in the 0.1 M aqueous solution of (a) LiCl, (b) NaCl, and (c) KCl. Scan rate is 100 mV/s.

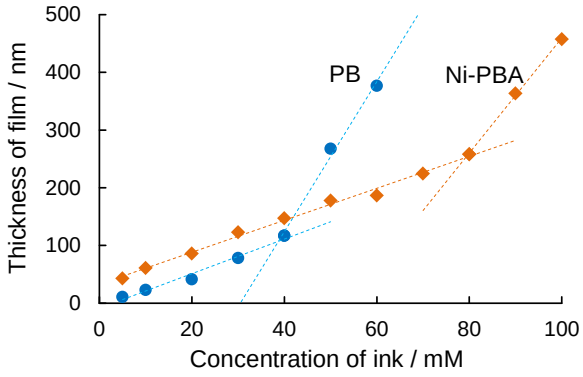

Fig. S9. Relationship between thicknesses of the low-temperature sintered SL films of PB and Ni-PBA NPs at 150 °C and concentrations of their inks.

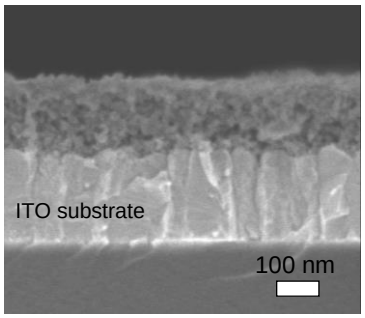

Fig. S10. SEM cross-section image of the low-temperature sintered DL film composed of the PB NP bottom layer (thickness, 20 nm; sintering temperature, 150 °C) and Ni-PBA NP top layer (150 nm; 120 °C). We could not distinguish the bottom layer of 20-nm thickness from the top one by our present SEM contrast technique because of the near atomic number electron configuration structures between Fe and Ni.

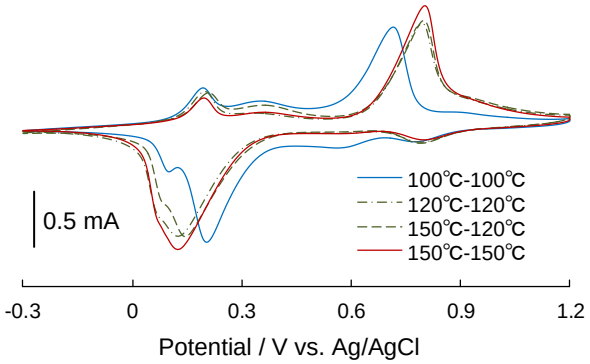

Fig. S11. Cyclic voltammograms of the low-temperature sintered DL film at various temperatures composed of the PB NP bottom layer (thickness, 20 nm) and Ni-PBA NP top layer (150 nm) in a 0.1 M aqueous solution of KCl. Right and left temperatures show sintering temperatures of the bottom and top layers, respectively. Scan rate is 100 mV/s.

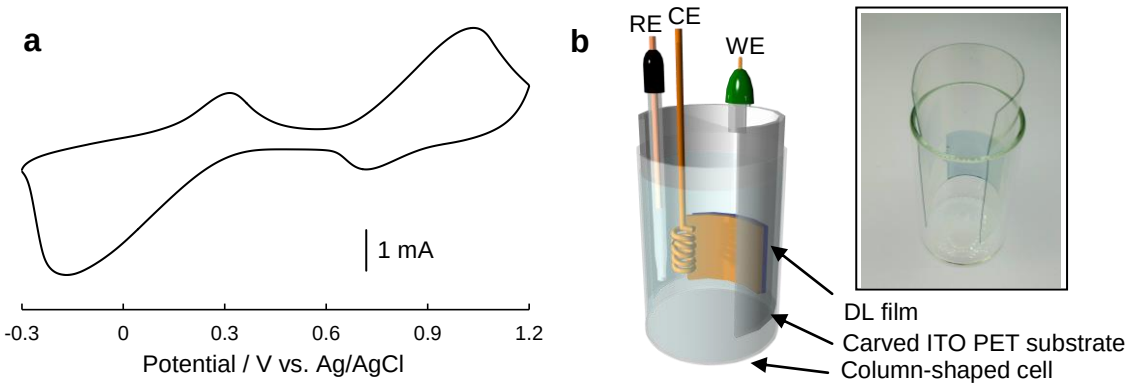

Fig. S12. (a) Cyclic voltammogram of the low-temperature sintered DL film composed of the PB NP bottom layer (thickness, 20 nm; sintering temperature, 150 °C) and Ni-PBA NP top layer (150 nm; 120 °C) on an ITO PET substrate in a 0.1 M aqueous solution of KCl. Scan rate is 100 mV/s. The observed cyclic voltammogram was broad compared with those in Fig. 3 and S11 because of the higher sheet resistance of the ITO PET substrate. (b) Measurement setup image for the cyclic voltammetry, where the ITO PET substrate was curved for demonstration of flexibility of the electron-rectifier device prototype (photograph).